

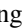
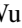
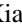



Photon blockade and single-photon generation with multiple quantum emitters

Mingyuan Chen , Jiangshan Tang , Lei Tang , Haodong Wu , and Keyu Xia *

College of Engineering and Applied Sciences, National Laboratory of Solid State Microstructures, Collaborative Innovation Center of Advanced Microstructures, Nanjing University, Nanjing 210093, China

 (Received 12 September 2021; revised 17 January 2022; accepted 13 July 2022; published 29 July 2022)

Generation and manipulation of single photons are at the heart of photon-based quantum information processing. An ensemble of quantum emitters (QEs) as a versatile light-matter interface are very promising for quantum technology such as quantum storage and repeater. However, it is commonly believed that many QEs are unable to create photon blockade and generate single photons with high purity due to the multiexcitation effect. Here, we show efficient photon blockade and single-photon generation with a few to ten QEs by suppressing multiexcitation with a detuned auxiliary cavity. Because the auxiliary cavity induces a strong dipole-dipole interaction among the QEs, these QEs can be treated as a two-level superatom. By coupling this superatom to another collecting cavity, efficient photon blockade with a high transmission is obtained. With the same setup, single-photon emission can also be achieved with yield and purity larger than 90% simultaneously even in the bad-cavity limit. Our method may open up a simple route to generate and manipulate single photons on demand.

DOI: [10.1103/PhysRevResearch.4.033083](https://doi.org/10.1103/PhysRevResearch.4.033083)

I. INTRODUCTION

The high-quality single-photon source plays a crucial role in quantum information processing such as secure quantum key distribution [1,2], quantum networking [3–5], and quantum computation [6–9]. Single photons have been generated from various platforms [10], including parametric driven nonlinear media [11–14] and single trapped quantum emitters (QEs) [15–28]. A single photon is heralded by detection of a scattered photon from an atomic ensemble after a single excitation is written in with a small success probability [29,30]. A modest photon blockade (PB) effect using an ensemble of atoms is predicted but associates with a vanishing low transmission [31]. The weak PB effect in an atomic ensemble is also proposed for lasing [32]. The PB effect based on the Kerr nonlinearity in atoms is also exploited to turn a heralded single-photon source to near-deterministic and thus surpasses the purity-yield limitation [33].

Cavity quantum electrodynamics (cQED) systems with a single QE have demonstrated the capability of achieving the PB effect in the strong coupling regime [15–18,31] and generating single photons with high yield. Nevertheless, realization of the strong coupling between a single QE and an optical cavity is extremely challenging in experiment. In comparison, trapping many atoms or few in a cavity can greatly simplify experimental implementation [34–36]. Despite this advantage, multiexcitation of atomic ensemble prevents one from realizing the strong PB and single-photon emission.

Emission and reabsorption of virtual photons between two atoms separate at a deep subwavelength distance causes the dipole-dipole interaction (DDI) [37–41]. For a very small distance, the near-field resonant DDI is paramount over relaxation process but typically difficult to achieve.

The DDI in atomic arrays has been extensively studied to induce the PB effect and generate single photons [42,43], especially in two-qubit cases [44–46]. However, the DDI needs to be stronger than the Dicke-state dissipation [38], which linearly increases with the atom number [37,38,47]. More importantly, the strongest virtual-photon-mediated DDI equal to the relaxation rate of the Dicke state has so far only been observed in two superconducting artificial atoms [48]. It is equally challenging as conducting a single-QE cQED system to achieve strong virtual-photon-mediated DDI. In contrast, a strong DDI among QEs can be induced with an optical cavity [41,49,50].

Rydberg atoms prepared via two-photon transitions can be used to circumvent the challenge in achieving a strong DDI. The strong dipolar interaction between Rydberg atoms induces shift of atomic energy levels and thus prevents multiexcitation of Rydberg atoms, giving rise to the so-called Rydberg blockade [51]. Rydberg blockade means that the one excited Rydberg atom prevents the neighboring atoms from excitation. As long as the Rydberg atoms reside within the blockade radius, the Rydberg blockade happens. The blockade effect increases with N owing to the cooperativity. This is an important advantage of single-photon generation utilizing Rydberg gases. Because of the weak multiphoton transition in Rydberg atoms, the coupling between an optical cavity and Rydberg atoms is typically small. Thus, to achieve an efficient photon collection and a strong PB with Rydberg atoms, the strong coupling of Rydberg atoms and an optical cavity needs to be developed.

To overcome the aforementioned challenges in the PB, we propose another approach to achieve the PB effect and

*keyu.xia@nju.edu.cn

Published by the American Physical Society under the terms of the Creative Commons Attribution 4.0 International license. Further distribution of this work must maintain attribution to the author(s) and the published article's title, journal citation, and DOI.

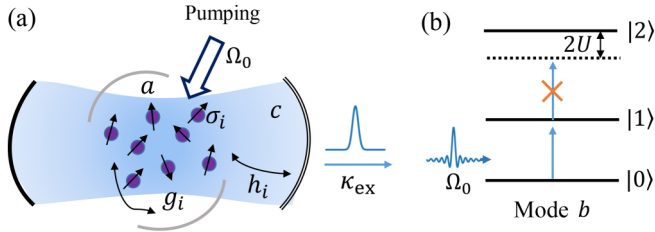


FIG. 1. (a) Schematics of our cQED system. The i th QEs (σ_i) couples to the auxiliary and one-side collecting cavities a and c with the coupling strengths g_i and h_i , respectively. A weak coherent light Ω_0 is used to pump the QEs emitting photons. The emitted photon couples out the collecting cavity with a rate κ_{ex} . (b) Level diagram of the equivalent superatom with a cavity-induced anharmonicity $2U$.

single-photon emission via the cavity-induced DDI among many two-level QEs.

The layout of this paper is as follows. In Sec. II we introduce the proposed scheme for realizing photon blockade and single-photon generation with multiple emitters in optical cavity QED system. In Sec. III we introduce the quantum trajectory method in detail, including the conditioned evolution of the quantum state and stochastic quantum jumps. In Sec. IV we discuss the photon blockade effect in our scheme, presenting both its advantages and limitations. In Sec. V we present results for single-photon generation. We numerically simulate Hanbury-Brown-Twiss experiment and discuss the effect of inhomogeneous broadening. An experimental implementation via cold ^{87}Rb atoms is proposed and analyzed in Sec. VI, with a brief conclusion and outlook on our paper in Sec. VII

II. SYSTEM AND MODEL

The schematic of our system is depicted in Fig. 1(a). N two-level QEs couples to an auxiliary cavity mode a with resonance frequency ω_a and to a collecting cavity mode c with resonance frequency ω_c . The coupling strengths between the j th QE and the cavity mode a (c) is g_j (h_j). We assume that these QEs have identical transition frequency ω_b and relaxation rate γ . The auxiliary cavity decays at a rate κ_a . The decay of the collecting cavity includes two contributions: the intrinsic decay κ_i and the extrinsic one κ_{ex} , yielding the total decay rate $\kappa_c = \kappa_i + \kappa_{\text{ex}}$. The treatment dividing the total decay into the intrinsic and extrinsic parts is useful for discussing the escape efficiency $\eta_{\text{esc}} = \kappa_{\text{ex}}/\kappa_c$ [33,52]. The escape efficiency is an important parameter to evaluate the performance of single-photon generation. The QEs are directly pumped with a coherent field $\Omega_0 = \sqrt{2\gamma P/\hbar\omega_p}$, which is related to the input power P , the driving frequency ω_p and the atomic relaxation rate γ . In the following we adopt natural units with $\hbar = 1$. We consider the two-level system with ground state $|g\rangle_j$ and excited state $|e\rangle_j$ for the j th QE. We introduce σ_j^\pm as respectively the raising and lowering operators acting on the j th QE.

In the rotating frame defined by a unitary transformation $U_1 = \exp\{i\omega_a(a^\dagger a + c^\dagger c + \frac{1}{2}\sum_{j=1}^N \sigma_j^z)t\}$, the system

Hamiltonian reads ($\hbar = 1$)

$$H = \Delta_{\text{ca}}c^\dagger c + \frac{1}{2}\Delta_{\text{ba}}\sum_{j=1}^N \sigma_j^z + \sum_{j=1}^N (g_j a^\dagger \sigma_j^- + g_j^* \sigma_j^+ a) + \sum_{j=1}^N (h_j c^\dagger \sigma_j^- + h_j^* \sigma_j^+ c) + i\Omega_0 \left(\sum_{j=1}^N \sigma_j^+ e^{i(\omega_p - \omega_a)t} - \sum_{j=1}^N \sigma_j^- e^{-i(\omega_p - \omega_a)t} \right) \quad (1)$$

with $\Delta_{\text{ca}} = \omega_c - \omega_a$ and $\Delta_{\text{ba}} = \omega_b - \omega_a$. This Hamiltonian is an extension of Dicke and Tavis-Cummings model [53,54]. We assume that the auxiliary cavity mode a and the QEs are largely detuned so that the mode a is unexcited, i.e., $\langle a^\dagger a \rangle \approx 0$.

To adiabatically eliminate the largely detuned cavity mode a , we apply the Schrieffer-Wolff transformation $U = e^S$ with $S = -\sum_j (g_j a^\dagger \sigma_j^- - g_j^* \sigma_j^+ a)/\Delta_{\text{ba}}$ to the many-body quantum system and keep terms up to the second order. [55,56]. This approximation is valid as long as $\Delta_{\text{ba}} \gg |g|$ [40,57]. The Hamiltonian in Eq. (1) becomes

$$H' = \Delta_{\text{ca}}c^\dagger c + \frac{1}{2}\Delta_{\text{ba}}\sum_{j=1}^N \sigma_j^z + \frac{1}{\Delta_{\text{ba}}} \left(\sum_{k=1}^N g_k \sigma_k^\dagger \sum_{j=1}^N g_j^* \sigma_j \right) + \sum_{j=1}^N (h_j c^\dagger \sigma_j^- + h_j^* \sigma_j^+ c) + i\Omega_0 \left(\sum_{j=1}^N \sigma_j^+ e^{i(\omega_p - \omega_a)t} - \sum_{j=1}^N \sigma_j^- e^{-i(\omega_p - \omega_a)t} \right). \quad (2)$$

The third term means the cavity-induced DDI [40,41,49,58,59]. To verify the validity of the adiabatic approximation, we have numerically calculated $\langle a^\dagger a \rangle$ and $g^2(0)$ versus the detuning Δ_{ba}/g . The result is shown in Fig. 5 in Appendix A. The adiabatic condition is satisfied for the parameters considered here. To further simplify this model, we assume the cavity-QE couplings are identical, i.e., $g_j = g_k = g$ and $h_j = h_k = h$. The effect of inhomogeneous coupling will be discussed later. With this treatment, we can define the collective spin operators $S_z = \frac{1}{2}\sum_j \sigma_j^z$, $S^+ = \sum_j \sigma_j^+$ and $S^- = \sum_j \sigma_j^-$. The Hamiltonian changes to

$$H = \Delta_{\text{ca}}c^\dagger c + \Delta_{\text{ba}}S^z + \frac{|g|^2}{2\Delta_{\text{ba}}}(S^+S^- + S^-S^+) + h(c^\dagger S^- + S^+c) + i\Omega_0(S^+ e^{i(\omega_p - \omega_a)t} - S^- e^{-i(\omega_p - \omega_a)t}). \quad (3)$$

With using the Holstein-Primakoff (H-P) transformation $S_z = b^\dagger b - N/2$, $S^+ = b^\dagger \sqrt{N - b^\dagger b}$, $S^- = \sqrt{N - b^\dagger b} b$ [60–62], the QE ensemble can be modeled as a bosonic mode b . In the following, we have used $S^+ \approx b^\dagger \sqrt{N}$ and $S^- \approx \sqrt{N} b$. This approximation is only valid when the excitation number $\langle b^\dagger b \rangle$ is low (see Appendix A). We further apply the unitary transformation $U_2 = \exp\{i(\omega_p - \omega_a)(c^\dagger c + b^\dagger b)t\}$ to the mode b and obtain the Hamiltonian in this new rotating frame

eventually reading as

$$\begin{aligned} \tilde{H} = & \tilde{\Delta}_c c^\dagger c + \tilde{\Delta}_b b^\dagger b + U(b^\dagger b)^2 + h'(b^\dagger c + bc^\dagger) \\ & + i\Omega(b^\dagger - b), \end{aligned} \quad (4)$$

with the detunings $\tilde{\Delta}_c = \omega_c - \omega_p$ and $\tilde{\Delta}_b = \Delta_{bp} + |g|^2(N - 1)/\Delta_{ba}$, and the collective driving $\Omega = \sqrt{N}\Omega_0$. The third term describes the collective nonlinear photon-photon interaction of the mode b resulting from the DDI among the QEs. The anharmonicity $U = |g|^2/\Delta_{ba}$ describes the collective nonlinearity strength. The modes c and b couple with a strength $h' = \sqrt{N}h$. The last term indicates the coherent driving of the mode b .

Note that the DDI causes an excitation-dependent energy shift $\delta E = U(b^\dagger b)^2$ to the mode b , see Fig. 1(b). Once the first excitation is loaded in the mode b , loading the second excitation needs an external energy $2U$. For the anharmonicity $2U > \gamma$, the excitation of high Fock states $|n \geq 2\rangle$ in mode b are greatly suppressed. We can treat the anharmonic cavity mode b as a two-level “superatom” only including the ground and first-excited states $|0\rangle$ and $|1\rangle$ [63], see Fig. 1(b). Thus, we attain a cQED system with a single superatom.

In our system, the QEs are off resonance from the cavity mode a . Owing to the anti-Purcell effect [64], a large QE-cavity detuning can suppress the decay of the N-QE collective states to $\Gamma = N\kappa_a g^2/(\kappa_a^2 + \Delta_{ba}^2) = N\gamma C/(1 + \Delta_{ba}^2/\kappa_a^2)$ with the cooperativity $C = g^2/\gamma\kappa_a$ [41,49,58,59,65]. We obtain the ratio of the collective nonlinearity to the decay

$$U/\Gamma = \frac{1}{N} \left(\frac{\kappa_a}{\Delta_{ba}} + \frac{\Delta_{ba}}{\kappa_a} \right). \quad (5)$$

This relation shows that a large nonlinearity U appears when $\kappa_a \gg \Delta_{ba}$. Thus, even if the auxiliary cavity is in the bad-cavity limit $\kappa_a \gg g$, a strong PB effect is available. This is the first key result of our cavity-QED protocol. Notice that for practical implementation, κ_a should not be too large and the single emitter dissipation rate γ is a small value. Thus, we choose a trade-off value $\Gamma = \gamma$. This protocol provides an advantage over previous PB schemes relying on the good-cavity limit in the optical regime. Driving the superatom with a coherent light field, we can, in principle, deterministically generate single photons because the anharmonicity causes the PB effect suppressing multiexcitation during photon emission. This is the second main discovery of this paper. Note that the ratio U/Γ is inversely proportional to N . As a result, the single-photon purity and yield decrease almost linearly as N increases. Nevertheless, the performance is still usable for up to ten atoms.

III. SIMULATION METHOD

The PB and photon emission can be investigated by solving the quantum master equation of density matrix $\rho(t)$,

$$\dot{\rho} = -i[\tilde{H}, \rho] + \sum_{j=1,2} \left[C_j \rho C_j^\dagger - \frac{1}{2} C_j^\dagger C_j \rho - \frac{1}{2} \rho C_j^\dagger C_j \right], \quad (6)$$

where the collapse operators $C_1 = \sqrt{\kappa_c}c$ and $C_2 = \sqrt{\Gamma}b$ respectively describe the annihilation of the modes c and b . The

feasibility of all applied parameter values will be discussed in the implementation part.

To numerically solve Eq. (6), we apply Monte Carlo quantum trajectory method [66–70]. The workflow of the quantum trajectory method is as follows. Supposing our state vector $|\psi(t)\rangle$ evolves from t to $t + \delta t$, a quantum trajectory evolves this ket vector according to the nonunitary Schrödinger equation

$$i \frac{d}{dt} |\psi(t)\rangle = H_e |\psi(t)\rangle, \quad (7)$$

where $H_e = H - i \sum_j C_j^\dagger C_j$ is the effective non-Hermitian Hamiltonian and $j = 1, 2$ labels the collapse operators. In our system, the specified Hamiltonian H_e is given by

$$\begin{aligned} H_e = & \tilde{H} - i\kappa_c c^\dagger c - i\gamma b^\dagger b \\ = & (\tilde{\Delta}_c - i\kappa) c^\dagger c + (\tilde{\Delta}_b - i\gamma) b^\dagger b + U(b^\dagger b^\dagger b b) \\ & + h'(c^\dagger b + b^\dagger c) + i\Omega(b^\dagger - b). \end{aligned} \quad (8)$$

This evolution is augmented by quantum jumps at random times with probabilities $\delta p = \sum_j \delta p_j = \sum_j \langle \psi(t) | C_j^\dagger C_j | \psi(t) \rangle \delta t$. If no jump occurs, the state vector evolves as $|\psi(t + \delta t)\rangle = \exp(-iH_e \delta t) |\psi(t)\rangle / (1 - \delta p)^{\frac{1}{2}}$. If one jump occurs, the non-Hermitian time evolution described by Eq. (7) is terminated and the corresponding wavefunction is projected and renormalized to

$$|\psi(t + \delta t)\rangle = \frac{C_j |\psi(t)\rangle}{\sqrt{\delta p_j / \delta t}}. \quad (9)$$

Then, the new state vector continues to evolve with H_e until it meets the next stochastic quantum jump or the simulation time finishes. This single stochastic evolution of the state vector is called one quantum trajectory. Note that the evolution of the quantum system is conditioned on event without detecting photons. The statistical averages of many quantum trajectories recover the solution of the master equation (6).

Unlike the quantum master equation, the quantum trajectory method is specially useful for studying the statistical properties of photons outside a cavity, characterizing a real detection process. The stochastic quantum jumps describe the situation that, e.g., one photon-emission event, is detected by a detector. While the non-Hermitian evolution described by Eq. (7) corresponds to the modification of the system state vector with a no-detection event. Therefore, the time evolution of each stochastic quantum trajectory can be completely reconstructed by an outside observer.

IV. PHOTON BLOCKADE WITH MULTIPLE EMITTERS

The PB effect means that emitting one photon in the cavity prohibits emission of following photons due to the system anharmonicity in energy. It can be characterized by the equal-time second-order correlation function $g^{(2)}(0) \equiv \langle c^{\dagger 2} c^2 \rangle / \langle c^\dagger c \rangle^2$. The PB happens when $g^{(2)}(0) < 1$. It only requires that the single-photon nonlinearity U is larger than the linewidth of mode b in our system, rather than the cavity mode as the conventional PB scheme. The transmission is also an important feature for the PB promising applications and is evaluated as $T = \gamma \kappa_{ex} \langle c^\dagger c \rangle / \Omega^2$ here.

To confirm the superatom picture discussed previously, we first derive a closed form of $g^{(2)}(0)$. We consider the decay terms of the QEs and the collecting cavity in the effective Hamiltonian equation (8). A general state takes the form $|\psi(t)\rangle = \sum_{n=0}^2 C_{n_1, n_2}(t) |n_1, n_2\rangle$, where n_1 and n_2 are respectively the collecting cavity photon number and the mode b excitation, and C_{n_1, n_2} the probability amplitude of state $|n_1, n_2\rangle$. Under the weak driving approximation ($\Omega \ll \gamma$), we truncate both modes up to state $|n=2\rangle$ although the mode b can be treated as a two-level superatom for large U . In this case, we can include the influence of the weakly excited states $|2\rangle$. Then the time-dependent Schrödinger equation $i|\dot{\psi}(t)\rangle = H_e|\psi(t)\rangle$ can be expanded as

$$\begin{aligned} i\dot{C}_{00} &= (\tilde{\Delta}_c - i\kappa)C_{00}, \\ i\dot{C}_{10} &= (\tilde{\Delta}_c - i\kappa)C_{10} + h'C_{01}, \\ i\dot{C}_{01} &= (\tilde{\Delta}_b - i\gamma)C_{01} + h'C_{10} + \Omega C_{00}, \\ i\dot{C}_{20} &= 2(\tilde{\Delta}_c - i\kappa)C_{20} + \sqrt{2}h'C_{11}, \\ i\dot{C}_{02} &= 2(\tilde{\Delta}_b - i\gamma)C_{02} + 2UC_{02} + \sqrt{2}h'C_{11} + \sqrt{2}\Omega C_{01}, \\ i\dot{C}_{11} &= (\tilde{\Delta}_b + \tilde{\Delta}_c - i(\kappa + \gamma))C_{11} \\ &\quad + \sqrt{2}h'(C_{20} + C_{02}) + \Omega C_{10}. \end{aligned} \quad (10)$$

The second-order correlation function approximates to

$$g^{(2)}(0) = \frac{\sum_n n(n-1)P_n}{(\sum_n nP_n)^2} \approx \frac{2P_2}{(P_1 + 2P_2)^2}, \quad (11)$$

where P_1 and P_2 are the single- and two-photon populations in photon wavefunctions. Because $P_1 \gg P_2$ under a weak pump, $g^{(2)}(0)$ can be further simplified to $g^{(2)}(0) \approx 2P_2/P_1^2 \approx 2|C_{2,0}|^2/|C_{1,0}|^4$. Then we can solve the Schrödinger equation $i|\dot{\psi}(t)\rangle = H_e|\psi(t)\rangle$ under a continuous wave (cw) driving and get an analytical expression for probability amplitude in steady state [71]. The coefficients $C_{1,0}$ and $C_{2,0}$ can be solved according to Eq. (10) as

$$C_{10} = \frac{h'\Omega}{(\tilde{\Delta}_c - i\kappa)(\tilde{\Delta}_b - i\gamma) - h'^2}, \quad (12)$$

$$C_{20} = \frac{D_1 h' \Omega C_{10}}{\tilde{\Delta}_b + \tilde{\Delta}_c - i(\kappa + \gamma) - D_2 h'^2},$$

where $D_1 = 1/(\tilde{\Delta}_c - i\kappa) - 1/(\tilde{\Delta}_b + U - i\gamma)$ and $D_2 = 1/(\tilde{\Delta}_c - i\kappa) + 1/(\tilde{\Delta}_b + U - i\gamma)$. On resonance, the function $g^{(2)}(0)$ eventually is given by

$$g^{(2)}(0) = \frac{\alpha_1(h^2 + \kappa_c\gamma)^2}{\alpha_2 h^4 + \alpha_3 h^2 + \alpha_4}, \quad (13)$$

where $\alpha_1 = U^2 + (\kappa_c - \gamma)^2$, $\alpha_2 = U^2 + (\kappa_c + \gamma)^2$, $\alpha_3 = \frac{1}{2}\kappa_c(\kappa_c + \gamma)(U^2 + \gamma^2 + 4\kappa_c\gamma)$, $\alpha_4 = \kappa_c^2(U^2 + \gamma^2)(\kappa_c + \gamma)^2$. In the limit of very large U , the correlation function reduces to

$$g^{(2)}(0) = \frac{(h^2 + \kappa_c\gamma)^2}{h^4 + 0.5\kappa_c^2 h^2 + \kappa_c^4}. \quad (14)$$

It is the correlation function of a cQED system embedded with a two-level QE. Taking $\{\kappa_c, \gamma, h', N\}/\kappa_i = \{61, 0.4, 2.0, 5\}$ in

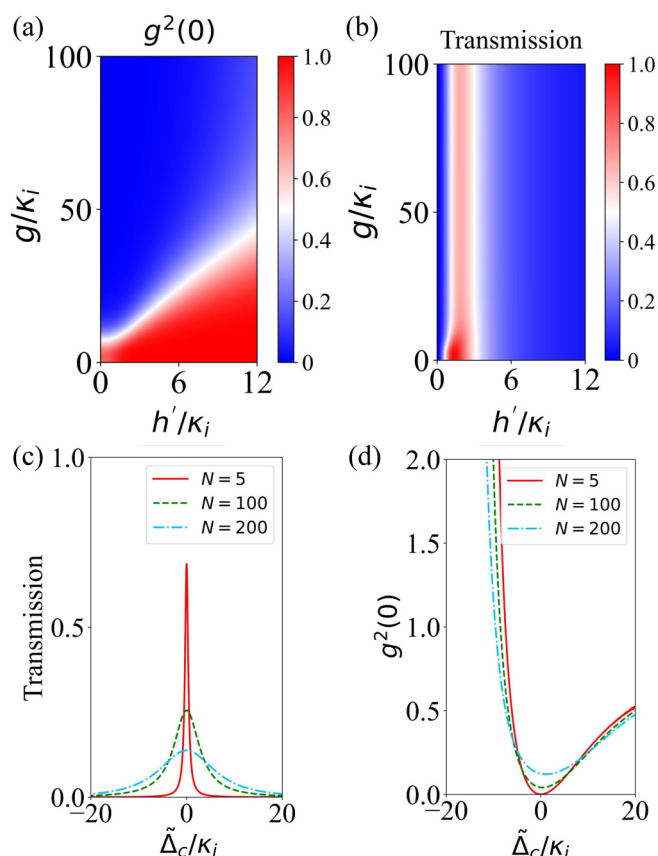


FIG. 2. (a) Equal-time second-order correlation function $g^{(2)}(0)$ and (b) transmission spectrum vs the coupling strengths g and h' . (c) The $g^{(2)}(0)$ and (d) transmission spectrum vs the detuning $\tilde{\Delta}_c$. Other parameters are $\{N, \kappa_{\text{ex}}, \gamma, h', g, \Delta_{\text{ba}}, \Omega\}/\kappa_i = \{5, 60, 0.4, 2.0, 46, 150, 0.16\}$.

the above equation, $g^{(2)}(0)$ reaches 3×10^{-5} . This clearly shows that higher levels $|n \geq 2\rangle$ are barely excited and only single photons can be emitted.

To study the full quantum dynamics of our system, we numerically solve Eq. (6) with the QuTiP quantum optics package [72] and truncate both modes c and b to Fock state $|5\rangle$. To provide an evaluation on performance in practical case, we take κ_i to normalize other parameters related to energy or frequency in numerical simulations. The collecting cavity is set to be resonant with the $|0\rangle \leftrightarrow |1\rangle$ transition of the mode b , i.e., $\tilde{\Delta}_c = \tilde{\Delta}_b$. We use a large extrinsic dissipation of the collecting cavity mode that $\kappa_{\text{ex}} = 60\kappa_i$ to guarantee a high escape efficiency $\eta_{\text{esc}} = \kappa_{\text{ex}}/\kappa_c$ [33,52]. We show the function $g^{(2)}(0)$ versus the coupling strengths g and h' in Fig. 2(a). It can be seen that $g^{(2)}(0)$ decreased monotonically with g because the nonlinearity U of the superatom is proportional to $|g|^2$. Moreover, $g^{(2)}(0)$ increases with h' . This is because a large h' results in higher level excitation of the superatom and thus multiphoton emission. The dependence of $g^{(2)}(0)$ on g and h' is consistent with our analytical results. Note that we obtain the ratio $P_2/P_1 = 2 \times 10^{-3}$ for $N = 5$, implying negligible multiphoton excitations in mode b . These numerical results strongly support that many QEs can be modeled as a two-level superatom.

Here, the collection cavity plays an important role in improving the transmission of single photons in photon blockade and the yield in single-photon generation. Without the collection cavity, the transmission will be vanishingly small as usual. On the other hand, the single-photon yield will also reduce to a small value, because the QEs very likely emits single photons into environment. Thus, we use this collection cavity to improve the performance of photon blockade and single-photon generation.

It can be seen from Fig. 2(a) that the function $g^{(2)}(0)$ can be improved from 1 to almost 0 as g (corresponding to U) increasing. In the limit of a large nonlinearity, our model simplifies to a cQED system consisting of a two-level superatom and a single collection cavity. When $h'/\kappa_c \rightarrow 0$, corresponding to the bad-cavity limit of the collection cavity, equation (13) reduces to

$$g^{(2)}(0) = \frac{(U^2 + (\kappa_c - \gamma)^2)\gamma^2}{[(U^2 + \gamma^2)(\kappa_c + \gamma)^2]}. \quad (15)$$

We can achieve a strong photon blockade effect. However, if the coupling of the QEs and the cavity mode c is weak, i.e., for a small h' , it can be seen from Fig. 2(b) that the transmission of the single-photon state vanishes as many previous schemes. Thus, one of the main advantages of our photon-blockade protocol losses. Therefore, we choose a tradeoff value of the ratio $h'/\kappa_c \sim 2.0$ for achieving high yield and purity simultaneously, see Fig. 2(b).

The cavity-induced DDI allows us to achieve a strong PB effect and high transmission simultaneously. As shown in Figs. 2(b) and 2(c), we obtain $g^{(2)}(0) = 1 \times 10^{-3}$ corresponding to a single-photon purity of 99.9% and a peak transmission of 0.68 for $N = 5$ when the cw coherent pump is near resonance with the collecting cavity, i.e., $\tilde{\Delta}_c \approx 0$. When more QEs are embedded in the cavity, e.g., $N = 100$ or 200, the purity and the transmission reduce. This can be understood from Eq. (4). The nonlinearity U is independent of N . But Loading more QEs enhances the coupling $h' = \sqrt{N}h$ and $\Omega = \sqrt{N}\Omega_0$. As a result, the PB effect becomes weaker. In stark contrast to previous paper [31], our scheme can achieve a strong PB and a large transmission simultaneously.

V. SINGLE-PHOTON EMISSION

By exciting the two-level superatom with a π pulse, we expect single-photon emission with high purity and yield simultaneously. We define the single-photon yield here as the probability of emitting a single photon after the system is driven by a π -area pump pulse. For our cQED system with a large U , after the superatom emits a single photon, it has to be excited again before emitting a subsequent photon. In this case, the possibility of multiphoton emissions is negligible and $g^{(2)}(0) \approx 0$ is obtainable.

To simulate photon emission in real experiments, we numerically solve Eq. (6) with the Monte Carlo quantum trajectory method provided by the QuTiP Python package [72]. This method allows us to calculate the probability of k -photon emissions denoted as P'_k ($k = 1, 2$). Obviously, P'_1

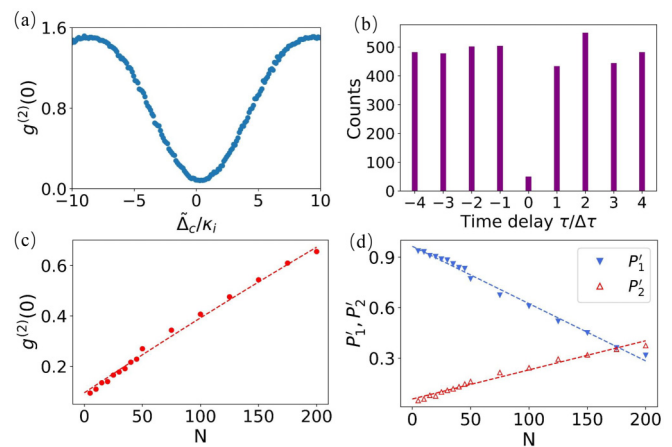


FIG. 3. Results of single photon emission with emitters. (a) Sweeping of detuning $\tilde{\Delta}_c$ vs two-photon correlation function. $g^{(2)}(0)$ reaches its minimum near resonance $\tilde{\Delta}_c = 0$. (b) HBT simulation of photon emission with 5000 quantum trajectories. $N = 5$ in (a) and (b). (c) $g^{(2)}(0)$ versus the number of QEs. (d) Single- and two-photon emission probability P_1 and P_2 vs N . Other parameters are $\{\kappa_{\text{ex}}, \gamma, h', g, \Delta_{\text{ba}}, \Omega\}/\kappa_i = \{60, 0.4, 2.0, 46, 150, 2.4\}$.

is the single-photon yield. This Monte Carlo method also enables us to evaluate the quantum statistics such as $g^{(2)}$ of photon wave functions outside the collecting cavity by simulating the Hanbury-Brown-Twiss (HBT) experiment [33,72].

The correlation function $g^{(2)}(0)$ versus the detuning $\tilde{\Delta}_c$ is shown in Fig. 3(a). When the π -pulse driving is on resonance, i.e., $\tilde{\Delta}_c = 0$, the function $g^{(2)}(0)$ is optimal and reaches $g^{(2)}(0) = 0.09$, corresponding to a purity >90%. The associating yield P_1 is also high, about 93%.

The time-delayed photon counts outside the collecting cavity can provide realistic photon statistics of fields in experimental observation. Simulation of HBT experiment presents the photon counts as a function of time delay, as shown in Fig. 3(b). Here, we numerically simulate the practical HBT experiment using two single-photon detectors to characterizing the single-photon nature for the following reasons. Firstly, the standard HBT scheme enables us to measure the quantum correlation between incident photons, while only a single detector cannot. Secondly, the HBT protocol does not require high photon-number-resolved detectors and is easy to implement experimentally. Another reason is, we aim to demonstrate a numerical method to simulate practical HBT experiment based on quantum trajectory. This method enables us to directly evaluate single-photon properties escaping off the optical cavity. This is an advantage over traditional simulation method calculating the in-cavity photons based on density matrix. (For more information, see Appendix C.) To do simulation, we divide the external decay of the collecting cavity into two collapse channels with equal rates $\kappa_{e1} = \kappa_{e2} = 30\kappa_i$ playing the role of a 50 : 50 beam splitter. These two channels are denoted as D_1 for time trigger and D_2 for stop. We input nine rectangle driving pulses with duration $\tau_p = 0.25\gamma^{-1}$ and interval $\Delta\tau = 5\gamma^{-1}$ corresponding to a repetition rate 0.2γ . This interval is long enough such that the collecting cavity can completely emit a photon outside. The emitted single-photon wavefunction is approximately a pulse exponentially decaying

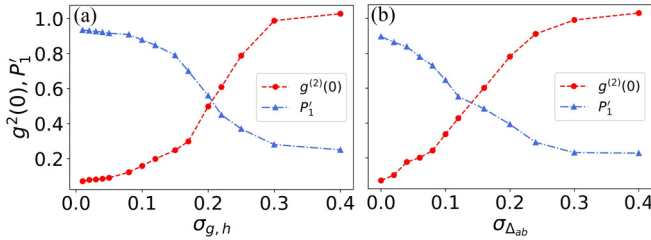


FIG. 4. Single-photon yield and purity vs (a) inhomogeneous broadening of the coupling strength and (b) emitter frequencies. The coupling strengths g_j and h_j in (a) are normally distributed around mean of $\bar{g}/\kappa_i = 46$ and $\bar{h}'/\kappa_i = 2.0$. The frequencies of emitters in (b) are also normally distributed with mean $\bar{\Delta}_{ba} = 150\kappa_i$. Other parameters are $\{N, \kappa_{ex}/\kappa_i, \gamma/\kappa_i, \Delta_{ba}/\kappa_i, \Omega/\kappa_i\} = \{5, 60, 0.4, 150, 2.4\}$.

with rate γ . If D_1 receives one photon within the i_{th} interval, followed by another “click” on D_2 within the $(i+k)_{th}$ interval, we consider this event as one count at $\tau = k\Delta\tau$. If the followed photon emission is still in the same detector, the count continues. As shown in Fig. 3(b), at zero time delay $\tau = 0$, we obtain 49 two-photon events over 5000 quantum trajectories, corresponding to $g^{(2)}(0) = 0.10 \pm 0.02$ [73]. This value of $g^{(2)}(0)$ is consistent with Fig. 3(a). This photon count simulation reflects photon statistics in real HBT experimental observation.

The yield and purity decrease as the number of QEs N increases, see Figs. 3(c) and 3(d), because the PB effect weakens. Increasing the number of QEs enhances the collective coupling strength $h' = \sqrt{N}h$ and the collective driving $\Omega = \sqrt{N}\Omega_0$. However, the nonlinearity U of the superatom remains unchanged. As a result, the multiphoton excitation increases. By fitting numerical results, we find the linear dependence of the purity and the yield on N : $P_1 = -0.0034N + 0.96$ and $P_2 = 0.00175N + 0.057$ for $N \leq 200$, leading to $g^{(2)}(0) = (0.0035N + 0.114)/(0.0001N + 1.074)^2 \sim 0.003N + 0.099$ (see dashed lines). These results imply that our system with N up to ten is well suitable for a single-photon source.

Note that a large coupling rate h' will cause Rabi oscillation between the superatom and the collection cavity mode. This may reduce the purity of the single photon and cause time-bin single photons [74].

The nonuniform amplitude distribution of the cavity field at different QE position may cause inhomogeneous broadening of the QE-cavity coupling. Here we investigate the dependence of single-photon yield and purity on the broadening of the coupling strengths g_j and h_j . To do so, we replace the Hamiltonian \hat{H} in the master equation with the many-body Hamiltonian given by Eq. (2) and solve the master equation. Limited by available computation resource, we consider a cQED system with $N = 10$. We assume that the randomly distributed couplings $\{g_j\}$ and $\{h_j\}$ have the same normal distribution with a standard derivation $\sigma_{g,h}$. Their mean values are $\bar{g} = 46\kappa_i$ and $\bar{h}' = 2.0\kappa_i$, respectively. The dependencies of the purity and the yield on $\sigma_{g,h}$ are shown in Fig. 4. As intuitive expectation, the purity and the yield decreases with the deviation $\sigma_{g,h}$. Nevertheless, we still can attain the purity and the yield larger than 90% [$P_1 > 0.9$, $g^2(0) < 0.1$] when

$\sigma_{g,h} < 0.08$. The coupling deviation has a small effect on single-photon emission in this case. As $\sigma_{g,h}$ further increases, the quality of the emitted single photon quickly deteriorates to useless. Thus, to obtain a high-quality single-photon source, we need to trap the many QEs in the cavities with a subwavelength size or an array of QEs separate by integer number of wavelengths to guarantee $\sigma_{g,h} < 0.08$ [34,42,75].

Our protocol can be extended to solid QEs like NV centers in a diamond in cryogenic environment. NV centers located on different sites in a diamond may experience randomized effective potentials and strain, leading to inhomogeneous energy level splitting [76–80]. To evaluate the influence of the inhomogeneous broadening in resonance frequency of QEs on the purity and yield, we numerically solve the master equation with Hamiltonian equation (2) for $N = 10$. To do so, we assume a normal distribution of the detuning Δ_{ba} with mean value $\bar{\Delta}_{ba} = 150\kappa_i$ and standard deviation $\sigma_{\Delta_{ba}}$. The results for the purity and yield are shown in Fig. 4(b). It can be seen that the purity and yield decrease with the increasing of $\sigma_{\Delta_{ba}}$. In comparison with the inhomogeneity of the coupling strengths, the performance of single-photon generation is strongly dependent on the broadening of the QE resonance frequency. To guarantee a usable performance of $P_1 > 0.9$, $g^2(0) < 0.1$, the standard variance $\sigma_{\Delta_{ba}}$ of the frequency broadening of the solid QEs needs to be smaller than 4%, equivalently ~ 15 times of the decay rate of NV centers. It is worth noting that this decay rate of NV centers can be narrowed by applying a small in-plane magnetic field [81]. Therefore, our protocol has the potential to be implemented on a solid-state platform.

VI. EXPERIMENTAL IMPLEMENTATION

Our scheme can be implemented by trapping many atoms in two Fabry-Perot cavities [5,57,82,83]. For the collecting cavity, we assume that the mirror M1 is coated with 99.85% antireflection layer and the mirror M2 has a relatively low reflectivity 90.5% as an output port [84,85]. We take this cavity length to be 5 mm. In this case, the intrinsic (extrinsic) decay rate κ_i (κ_{ex}) of the collecting cavity can be calculated as $2\pi \times 7.2$ MHz ($2\pi \times 450$ MHz). The escape efficiency can reach $\eta_{esc} = 98.4\%$. Many ^{87}Rb atoms is used to create the nonlinearity. We can use the D1 lines $|5^2S_{1/2}, F = 2\rangle \rightarrow |5^2P_{1/2}, F' = 2\rangle$ with decay rate $\gamma = 2\pi \times 3$ MHz and transition wavelength $\lambda = 780.2$ nm. The auxiliary cavity can be a fiber Fabry-Perot cavity. The optimal mode volume for the fiber Fabry-Perot cavity can be down to $5.5\lambda^3$ [86], leading to the atom-cavity coupling strength up to $g = 2\pi \times 2.2$ GHz. We choose the cavity length of $25 \mu\text{m}$ and obtain $g = 2\pi \times 325$ MHz. It is reasonable to choose the coupling between atoms and the collecting cavity to be $h' = 2\pi \times 15$ MHz for $N = 5$. The auxiliary cavity can be a “bad” cavity with both mirrors having low reflectivity of 77%, yielding a decay rate of $\kappa_a \approx 198$ GHz and a quality factor $Q \approx 1200$. Then, we obtain the single-photon yield of $P_1 = 93\%$ and the purity of 90%. If a π -area driving pulse train with repeating rate ~ 3.7 MHz is applied to the QEs, we can near deterministically generate single photons with a rate of 3.4 MHz. Our scheme can also be realized on a chip by using photonic crystal cavities embedded with quantum dots [57,87]. The intrinsic dissipation of the self-assembled InAs/GaAs is

$\gamma = 2\pi \times 0.1 \text{ GHz}$ [88]. In this setup, the ratio of the non-linearity U to the quantum dot dissipation can be improved. Thus, we can expect a single-photon source with higher yield and purity and repetition rate of 125 MHz can be attained in such chip-compatible system.

VII. CONCLUSIONS

We have proposed a near-deterministic single-photon source with many QEs. Our scheme uses a largely detuned auxiliary cavity to induce a strong DDI in the QEs and thus create an effective cQED system with a single two-level superatom. With this system, we achieve the strong PB effect and obtain single-photon emission with high purity and yield. Our scheme paves the way for exploiting many QEs for single-photon source and may greatly simplify photon-based quantum information processing.

ACKNOWLEDGMENTS

K.X. thanks the support of the National Key R&D Program of China (Grants No. 2017YFA0303703, No. 2019YFA0308700 and No. 2019YFA0308704), the National Natural Science Foundation of China (Grants No. 11874212 and No. 11890704), and the Program for Innovative Talents and Teams in Jiangsu (Grant No. JSSCTD202138). This work is also supported by the High Performance Computing Center of Nanjing University for allowing the numerical calculation on its blade cluster system.

APPENDIX A: DERIVATION OF EFFECTIVE HAMILTONIAN

The original Hamiltonian of our system is

$$\begin{aligned}
 H = & \omega_c c^\dagger c + \omega_a a^\dagger a + \frac{1}{2} \omega_a \sum_j \sigma_j^z + \sum_j (g_j a^\dagger \sigma_j^- + g_j^* \sigma_j^+ a) \\
 & + \sum_j (h_j c^\dagger \sigma_j^- + h_j^* \sigma_j^+ c) + i\Omega_0 \\
 & \times \left(\sum_j \sigma_j^\dagger e^{i\omega_p t} - \sum_j \sigma_j e^{-i\omega_p t} \right), \tag{A1}
 \end{aligned}$$

where $c(c^\dagger)$ is the collecting cavity mode, the $a(a^\dagger)$ is the auxiliary cavity mode and σ_j^\pm is the transition operator of the j th emitter. The last two terms represent couplings between the quantum emitters and the two cavities. In the rotating frame defined by a unitary transformation $U_1 = \exp(i\omega_a(c^\dagger c + a^\dagger a + \frac{1}{2}\omega_a \sum_j \sigma_j^z)t)$, the Hamiltonian reads

$$\begin{aligned}
 H' = & U_1 H U_1^{-1} + i \frac{\partial U_1}{\partial t} U_1^\dagger \\
 = & \Delta_{ca} c^\dagger c + \frac{1}{2} \Delta_{ba} \sum_j \sigma_j^z + \sum_j (g_j a^\dagger \sigma_j^- + g_j^* \sigma_j^+ a) \\
 & + \sum_j (h_j c^\dagger \sigma_j^- + h_j^* \sigma_j^+ c) \\
 & + i\Omega_0 \left(\sum_j \sigma_j^\dagger e^{i(\omega_p - \omega_a)t} - \sum_j \sigma_j e^{-i(\omega_p - \omega_a)t} \right). \tag{A2}
 \end{aligned}$$

Here, $\Delta_{ca} = \omega_c - \omega_a$ and $\Delta_{ba} = \omega_b - \omega_a$. Then we apply the transformation $U_2 = e^S$ to Hamiltonian of Eq. (2), where $S = \frac{1}{\Delta} \sum_j (g_j a^\dagger \sigma_j^- - g_j^* \sigma_j^+ a)$. It can be clearly seen that only the second and third terms of Eq. (2) change under this transformation, so we denote $H'_1 \equiv \frac{1}{2} \Delta_{ba} \sum_j \sigma_j^z$ and $V'_1 \equiv \sum_j (g_j a^\dagger \sigma_j^- + g_j^* \sigma_j^+ a)$ for simplicity. Substituting the BCH formula,

$$e^A B e^{-A} = B + [A, B] + \frac{1}{2!} [A, [A, B]] + \dots, \tag{A3}$$

into Eq. (2), we have

$$\begin{aligned}
 [S, H'_1] = & -\frac{1}{2} \sum_j (g_j a^\dagger [\sigma_j^-, \sigma_j^z] - g_j^* [\sigma_j^+, \sigma_j^z] a) \\
 = & -\sum_j (g_j a^\dagger \sigma_j^- + g_j^* \sigma_j^+ a) = -V'_1. \tag{A4}
 \end{aligned}$$

This condition implies that our transformation resembles Schrieffer-Wolff transformation in condensed matter system. The transformed term $H'_1 + V'_1$ becomes

$$\begin{aligned}
 e^{+S} (H'_1 + V'_1) e^{-S} = & H'_1 + \frac{1}{2} [S, V'_1] \\
 = & \frac{1}{2} \Delta_{ba} \sum_j \sigma_j^z - \frac{1}{2\Delta_{ba}} \sum_k \sum_j [g_k a^\dagger \sigma_k^- - g_k^* \sigma_k^+ a, g_j a^\dagger \sigma_j^- + g_j^* \sigma_j^+ a] \\
 = & \frac{1}{2} \Delta_{ba} \sum_j \sigma_j^z + \frac{1}{2\Delta_{ba}} \left(\sum_j g_j^* \sigma_j^+ \sum_k g_k \sigma_k^- + \sum_j g_j \sigma_j^- \sum_k g_k^* \sigma_k^+ \right) + \frac{|g|^2}{\Delta_{ba}} \sum_j a^\dagger a \sigma_j^z. \tag{A5}
 \end{aligned}$$

We truncate the transformed Hamiltonian up to second order and then get

$$\begin{aligned}
 H'' = & \Delta_{ca} c^\dagger c + \frac{1}{2} \Delta_{ba} \sum_j \sigma_j^z + \frac{1}{2\Delta_{ba}} \left(\sum_j g_j^* \sigma_j^+ \sum_k g_k \sigma_k^- + \sum_j g_j \sigma_j^- \sum_k g_k^* \sigma_k^+ \right) \\
 & + \frac{|g|^2}{\Delta_{ba}} \sum_j a^\dagger a \sigma_j^z + \sum_j (h_j c^\dagger \sigma_j^- + h_j^* \sigma_j^+ c) + i\Omega_0 \left(\sum_j \sigma_j^\dagger e^{i(\omega_p - \omega_a)t} - \sum_j \sigma_j e^{-i(\omega_p - \omega_a)t} \right). \tag{A6}
 \end{aligned}$$

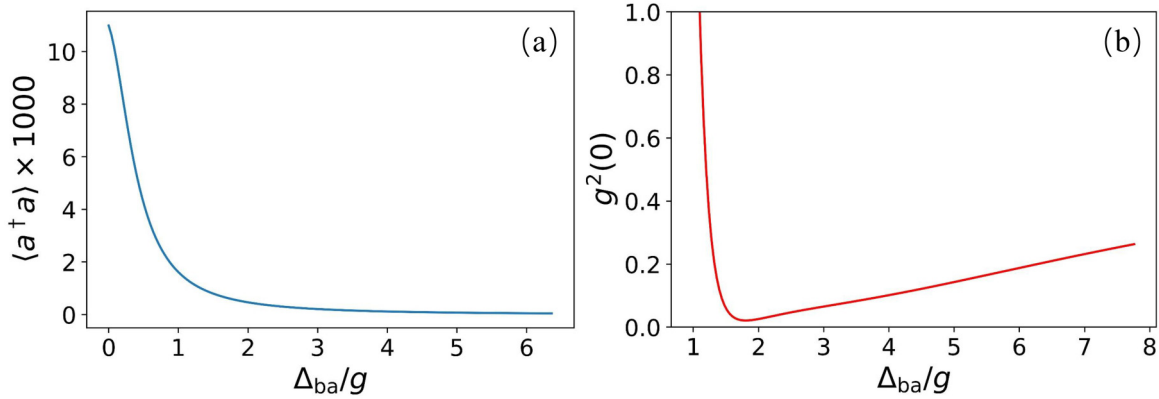


FIG. 5. The calculation of mean excitation $\langle a^\dagger a \rangle$ (a) and $g^{(2)}(0)$ (b) function vs detuning Δ_{ba}/g . The excitation of mode a decreases exponentially with large Δ_{ba}/g . The $g^{(2)}(0)$ function experience a drastic drop with $\Delta_{ba}/g < 2$ and slowly increases afterwards.

Here, the auxiliary cavity and the QEs are off resonance, i.e., $\Delta_{ba} \gg |g|$, so that the mode a is barely excited, i.e., $\langle a^\dagger a \rangle \approx 0$. In this case, the stark-shift related term $\frac{|g|^2}{\Delta_{ba}} \sum_j a^\dagger a \sigma_j^z$ can be neglected for simplicity. Introducing the collective spin operator $S^+ = \sum_j \sigma_j^+$, $S^- = \sum_j \sigma_j^-$, $S^z = \frac{1}{2} \sum_j \sigma_j^z$, we obtain the Hamiltonian H''

$$H'' = \Delta_{ca} c^\dagger c + \Delta_{ba} S^z + \frac{|g|^2}{2\Delta_{ba}} (S^+ S^- + S^- S^+) + h(c^\dagger S^- + S^+ c) + i\Omega_0 (S^+ e^{i(\omega_p - \omega_a)t} - S^- e^{-i(\omega_p - \omega_a)t}). \quad (\text{A7})$$

Under the Holstein-Primakoff transformation $S^z = b^\dagger b - \frac{N}{2}$, $S^+ = b^\dagger \sqrt{N - b^\dagger b}$, $S^- = \sqrt{N - b^\dagger b} b$, the Hamiltonian becomes

$$H = \Delta_{ca} c^\dagger c + \left(\Delta_{ba} + N \frac{|g|^2}{\Delta_{ba}} \right) b^\dagger b + \frac{|g|^2}{\Delta_{ba}} b^\dagger b^\dagger b b + h(c^\dagger \sqrt{N - b^\dagger b} b + b^\dagger \sqrt{N - b^\dagger b} c) + i\Omega_0 (b^\dagger \sqrt{N - b^\dagger b} e^{i(\omega_p - \omega_a)t} - \sqrt{N - b^\dagger b} b e^{-i(\omega_p - \omega_a)t}). \quad (\text{A8})$$

We assume that $S^+ = b^\dagger \sqrt{N - b^\dagger b} \approx \sqrt{N} b^\dagger$, $S^- = \sqrt{N - b^\dagger b} b \approx \sqrt{N} b$ for large N . Then the Hamiltonian can be simplified to

$$H = \Delta_{cp} c^\dagger c + \left(\Delta_{bp} + \frac{|g|^2}{\Delta_{ba}} (N - 1) \right) b^\dagger b + \frac{|g|^2}{\Delta_{ba}} (b^\dagger b)^2 + h'(b^\dagger c + b c^\dagger) + i\Omega(b^\dagger - b) = \tilde{\Delta}_c c^\dagger c + \tilde{\Delta}_b b^\dagger b + U(b^\dagger b)^2 + h'(b^\dagger c + c^\dagger b) + i\Omega(b^\dagger - b), \quad (\text{A9})$$

where the detunings $\tilde{\Delta}_c = \omega_c - \omega_p$ and $\tilde{\Delta}_b = \Delta_{bp} + |g|^2(N - 1)/\Delta_{ba}$. The collective coupling strength is $h' = \sqrt{N}h$ and the collective driving is $\Omega = \sqrt{N}\Omega_0$. We obtain the Hamiltonian given by Eq. (3) in the main text.

Below, we validate the adiabatic elimination of the auxiliary cavity mode. Using the original Hamiltonian equation (1), we investigate the dependence of the mean excitation number $\langle a^\dagger a \rangle$ on the detuning Δ_{ba} , as shown in Fig. 5(a). The excitation of cavity mode a decreases exponentially and drops to a vanishing small value 2×10^{-4} at $\Delta_{ba}/g = 3$. Thus, it is

reasonable to adiabatically eliminate the auxiliary cavity by considering it in its quantum ground state [40,57].

We also study the $g^{(2)}(0)$ function versus detuning Δ_{ba} , see Fig. 5(b). It first drops to a minimal value quickly as the detuning increases. This indicates the collection cavity a is barely excited and the auxiliary cavity-atoms system can be treated as a single superatom. The function $g^{(2)}(0)$ linearly increases afterwards. This is because the nonlinearity $U = |g|^2/\Delta_{ba}$ decreases. These results also confirm the validity of the adiabatic elimination.

APPENDIX B: COMPARISON BETWEEN ANALYTICAL AND NUMERICAL RESULTS OF $g^{(2)}(0)$

The analytical expression of correlation function on resonance condition, i.e., $\tilde{\Delta}_c = \tilde{\Delta}_b = 0$, is expressed as

$$g^{(2)}(0) = \frac{\alpha_1 (h^2 + \kappa\gamma)^2}{\alpha_2 h^4 + \alpha_3 h^2 + \alpha_4}, \quad (\text{B1})$$

where $\alpha_1 = U^2 + (\kappa - \gamma)^2$, $\alpha_2 = U^2 + (\kappa + \gamma)^2$, $\alpha_3 = \frac{1}{2}\kappa(U^2 + \gamma^2 + 4\kappa\gamma)(\kappa + \gamma)$, $\alpha_4 = \kappa^2(U^2 + \gamma^2)(\kappa + \gamma)^2$. As can be seen in Figs. 6(a) and 6(b), our analytical results fit well with the quantum trajectory simulation for small h' and large U . The correlation function $g^{(2)}(0)$ increases monotonically with h' and decreases with U . However, when h' is stronger, the analytical results deviate from numerical results. This is because the superatom is more probable to be excited to higher energy levels due to strong Rabi oscillation between the collecting cavity and the superatom. This result is not established as well when U/Γ is not large enough. In both cases, the superatom can no longer be treated as a two-level system and the weak-pump approximation $C_{00} \gg C_{10} \gg C_{20}$ is not valid anymore.

APPENDIX C: QUANTUM TRAJECTORY SIMULATION OF THE HBT EXPERIMENT

Quantum trajectory (QT) method provides an effective manner to simulate the photon statistics of the output field. This photon statistics is hard to simulate by directly solving the master equation of the system. The detailed discussion on the QT have been provided by Ref. [66] and Appendix seven

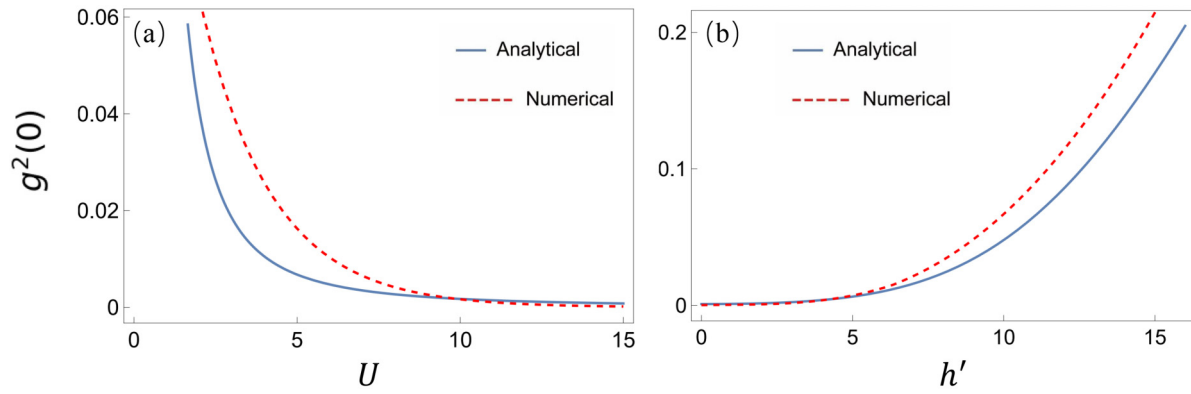


FIG. 6. Comparison between analytical and numerical results. The analytical results are plotted with Eq. (B1) and the numerical results are obtained by solving the master equation (4) in the main text. (a) $g^{(2)}(0)$ as a function of U . (b) $g^{(2)}(0)$ as a function of h' . Our analytical results fit well with numerical result when h' is small and U is large. The parameters discussed in the main text ($h' = 2.0\kappa_i$, $U = 14.1\kappa_i$) lies exactly in this region. Outside this region, the deviation becomes large. The other parameters are consistent with the main text.

of Ref. [33]. Here we only emphasize some key points. In the QT, if a single photon escapes from the cavity within a small time interval $\delta\tau$, then the state of the system will undergo a jump. After the jump, the system continues to evolve according to the Schrödinger equation.

This calculated system state as a function of time is called a quantum trajectory. We assume that there is a photon detector outside the collecting cavity that has the ability to tell whether or not a photon has been emitted. Therefore, in each QT simulation, the number of jumps of the system state corresponds to the number of photon events detected by the out-of-cavity detector. The desired density matrix as a function of time may be calculated by averaging over many simulated trajectories.

In our system, different cases of the quantum trajectories are plotted in Figs. 7(a)–7(c). In Fig. 7(a), no jump occurs, indicating that this state is the vacuum state. In Fig. 7(b), one jump occurs, which is the sign of single-photon emission from the cavity at time t_i . In Fig. 7(c), two jumps occur, which imply two-photon emission event subsequently happening at t_j and t_k . The moment of photon-emission event and the channels they emit through are recorded in QT simulation [72]. The average photon number outside the cavity over 1000 trajectories is shown in Fig. 7(d). The photon fully escapes after $\gamma t = 3$.

In the HBT simulation, we first set two dissipation channels with collapse rates $\kappa_{e1} = \kappa_{e2} = \kappa_{ex}/2$. These two channels

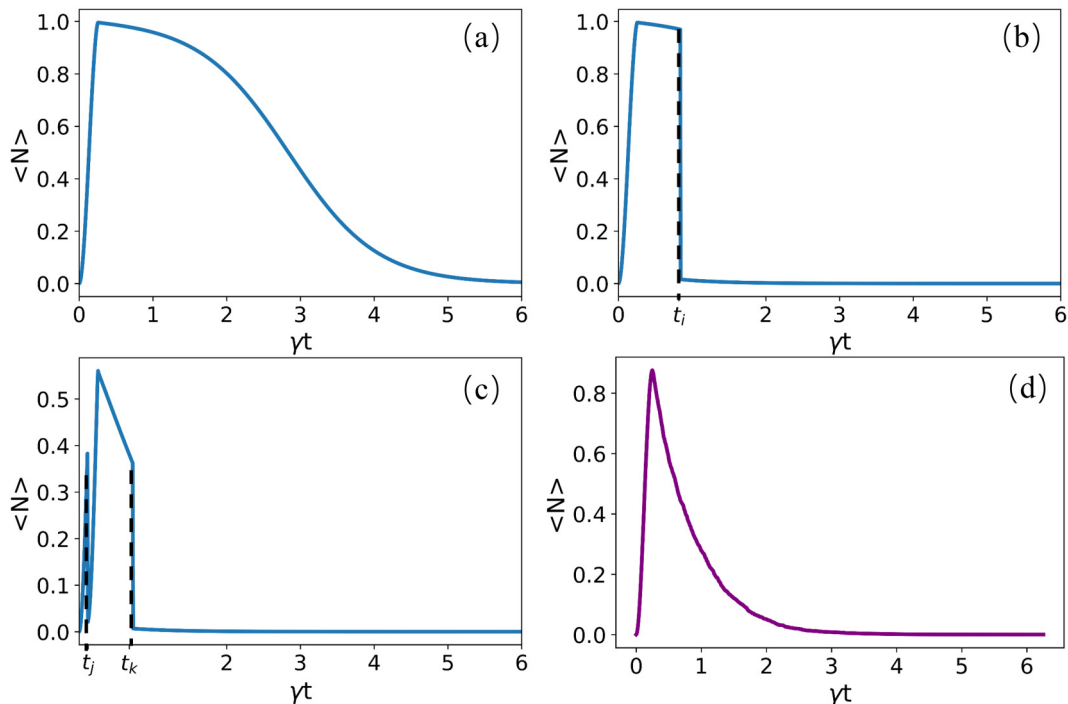


FIG. 7. Simulation of the output photons with one π pulse in our system, where the x axis represents the photon decay time in the cavity and the ordinate represents the average number of photons in the cavity. [(a),(b),(c)] Single-trajectory photon number for zero-, one-, and two-photon quantum jumps occurring within one pulse, respectively. (d) Average of over 1000 trajectories in the simulation.

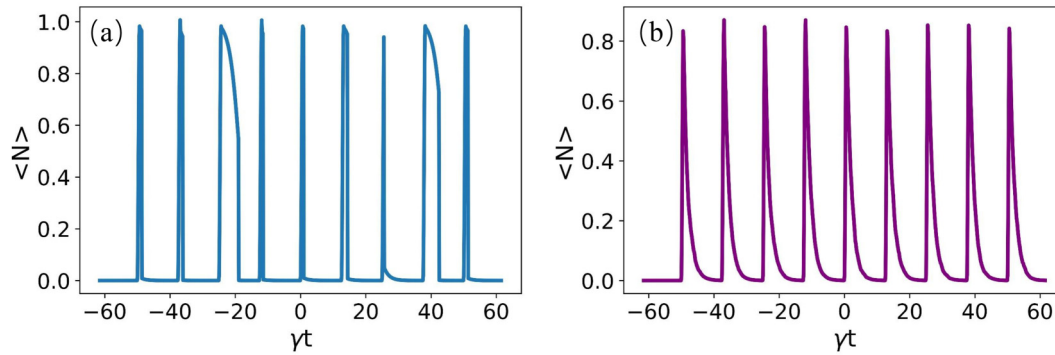


FIG. 8. Simulation of the output photons in the HBT simulation for nine input pulses with duration $\tau_0 \approx 0.25\gamma^{-1}$ and an interval $\Delta\tau = 5\gamma^{-1}$. (a) Photon numbers in a single trajectory. (b) Photon numbers averaged over 5000 trajectories.

serve as a 50 : 50 beam splitter. We input nine rectangular pulses with duration $\tau_0 \approx 0.25\gamma^{-1}$. Each pulse is separated by an interval $\Delta\tau = 5\gamma^{-1}$ to ensure no overlap (“wrong”) counting. One of the trajectory in the simulation is shown in Fig. 8(a). We can see that each of the pulse only “jumps” once. It indicates that nine single photons are emitted from the cavity in this trial. Figure 8(b) is the average of 5000 trajectories. After QT simulations are done, a set of lists are given. These lists record the time and channels for the photon-emission events in each QT [72]. We then sort out this set of results and divide them into two groups, labeling as D_1 and D_2 . For example, $D_1[x]$ contains all the moments

of the photon emission through the channel κ_{e1} in the x_{th} quantum trajectory. Then we can apply the counting procedure described in the main text in each trajectory. That is to say, we search the first incident photon in $D_1[x]$ and mark it as the “start” of one counting procedure. If $D_1[x]$ receives one photon within the i th interval, followed by another “click” on $D_2[x]$ within the $(i+k)$ th interval, we consider this event as one count in $\tau = k\Delta\tau$. If the followed photon emission is still in the same detector, the count continues. After summing over all the counts in each trajectory, we get the distribution result shown in the Fig. 3(b) of the main text.

-
- [1] V. Scarani, H. Bechmann-Pasquinucci, N. J. Cerf, M. Dušek, N. Lütkenhaus, and M. Peev, The security of practical quantum key distribution, *Rev. Mod. Phys.* **81**, 1301 (2009).
- [2] P. W. Shor and J. Preskill, Simple Proof of Security of the BB84 Quantum Key Distribution Protocol, *Phys. Rev. Lett.* **85**, 441 (2000).
- [3] H. J. Kimble, The quantum internet, *Nature (London)* **453**, 1023 (2008).
- [4] S. Ritter, C. Nölleke, C. Hahn, A. Reiserer, A. Neuzner, M. Uphoff, M. Mücke, E. Figueroa, J. Bochmann, and G. Rempe, An elementary quantum network of single atoms in optical cavities, *Nature (London)* **484**, 195 (2012).
- [5] M. Brekenfeld, D. Niemietz, J. D. Christesen, and G. Rempe, A quantum network node with crossed optical fibre cavities, *Nat. Phys.* **16**, 647 (2020).
- [6] A. Steane, Quantum computing, *Rep. Prog. Phys.* **61**, 117 (1998).
- [7] M. A. Nielsen and I. L. Chuang, *Quantum Computation and Quantum Information* (Cambridge University Press, Cambridge, 2010)
- [8] D. P. DiVincenzo, Quantum computation, *Science* **270**, 255 (1995).
- [9] K. Xia, M. Johnsson, P. L. Knight, and J. Twamley, Cavity-Free Scheme for Nondestructive Detection of a Single Optical Photon, *Phys. Rev. Lett.* **116**, 023601 (2016).
- [10] M. D. Eisaman, J. Fan, A. Migdall, and S. V. Polyakov, Invited review article: Single-photon sources and detectors, *Rev. Sci. Instrum.* **82**, 071101 (2011).
- [11] E. A. Goldschmidt, M. D. Eisaman, J. Fan, S. V. Polyakov, and A. Migdall, Spectrally bright and broad fiber-based heralded single-photon source, *Phys. Rev. A* **78**, 013844 (2008).
- [12] X.-S. Ma, S. Zotter, J. Kofler, T. Jennewein, and A. Zeilinger, Experimental generation of single photons via active multiplexing, *Phys. Rev. A* **83**, 043814 (2011).
- [13] C.-H. Yuan, L. Q. Chen, Z. Y. Ou, and W. Zhang, Generation of frequency-multiplexed entangled single photons assisted by entanglement, *Phys. Rev. A* **83**, 054302 (2011).
- [14] S. Li, X. Pan, Y. Ren, H. Liu, S. Yu, and J. Jing, Deterministic Generation of Orbital-Angular-Momentum Multiplexed Tripartite Entanglement, *Phys. Rev. Lett.* **124**, 083605 (2020).
- [15] J. McKeever, A. Boca, A. D. Boozer, R. Miller, J. R. Buck, A. Kuzmich, and H. J. Kimble, Deterministic generation of single photons from one atom trapped in a cavity, *Science* **303**, 1992 (2004).
- [16] B. Darquié, M. P. A. Jones, J. Dingjan, J. Beugnon, S. Bergamini, Y. Sortais, G. Messin, A. Browaeys, and P. Grangier, Controlled single-photon emission from a single trapped two-level atom, *Science* **309**, 454 (2005).
- [17] M. Hennrich, T. Legero, A. Kuhn, and G. Rempe, Photon statistics of a non-stationary periodically driven single-photon source, *New J. Phys.* **6**, 86 (2004).
- [18] A. Kuhn, M. Hennrich, and G. Rempe, Deterministic Single-Photon Source for Distributed Quantum Networking, *Phys. Rev. Lett.* **89**, 067901 (2002).
- [19] D. L. Moehring, P. Maunz, S. Olmschenk, K. C. Younge, D. N. Matsukevich, L. M. Duan, and C. Monroe, Entanglement of

- single-atom quantum bits at a distance, *Nature (London)* **449**, 68 (2007).
- [20] S. Gerber, D. Rotter, M. Hennrich, R. Blatt, F. Rohde, C. Schuck, M. Almendros, R. Gehr, F. Dubin, and J. Eschner, Quantum interference from remotely trapped ions, *New J. Phys.* **11**, 013032 (2009).
- [21] B. Lounis and W. E. Moerner, Single photons on demand from a single molecule at room temperature, *Nature (London)* **407**, 491 (2000).
- [22] C. Brunel, B. Lounis, P. Tamarat, and M. Orrit, Triggered Source of Single Photons based on Controlled Single Molecule Fluorescence, *Phys. Rev. Lett.* **83**, 2722 (1999).
- [23] C. Santori, M. Pelton, G. Solomon, Y. Dale, and Y. Yamamoto, Triggered Single Photons from a Quantum Dot, *Phys. Rev. Lett.* **86**, 1502 (2001).
- [24] R. B. Patel, A. J. Bennett, I. Farrer, C. A. Nicoll, D. A. Ritchie, and A. J. Shields, Two-photon interference of the emission from electrically tunable remote quantum dots, *Nat. Photonics* **4**, 632 (2010).
- [25] Y.-M. He, H. Wang, C. Wang, M.-C. Chen, X. Ding, J. Qin, Z.-C. Duan, S. Chen, J.-P. Li, R.-Z. Liu *et al.*, Coherently driving a single quantum two-level system with dichromatic laser pulses, *Nat. Phys.* **15**, 941 (2019).
- [26] H. Wang, Y.-M. He, T.-H. Chung, H. Hu, Y. Yu, S. Chen, X. Ding, M.-C. Chen, J. Qin, X. Yang *et al.*, Towards optimal single-photon sources from polarized microcavities, *Nat. Photonics* **13**, 770 (2019).
- [27] R. Brouri, A. Beveratos, J.-P. Poizat, and P. Grangier, Photon antibunching in the fluorescence of individual color centers in diamond, *Opt. Lett.* **25**, 1294 (2000).
- [28] H. Bernien, L. Childress, L. Robledo, M. Markham, D. Twitchen, and R. Hanson, Two-Photon Quantum Interference from Separate Nitrogen Vacancy Centers in Diamond, *Phys. Rev. Lett.* **108**, 043604 (2012).
- [29] C. W. Chou, S. V. Polyakov, A. Kuzmich, and H. J. Kimble, Single-Photon Generation from Stored Excitation in an Atomic Ensemble, *Phys. Rev. Lett.* **92**, 213601 (2004).
- [30] D. N. Matsukevich, T. Chanelière, S. D. Jenkins, S.-Y. Lan, T. A. B. Kennedy, and A. Kuzmich, Deterministic Single Photons via Conditional Quantum Evolution, *Phys. Rev. Lett.* **97**, 013601 (2006).
- [31] R. Trivedi, M. Radulaski, K. A. Fischer, S. Fan, and J. Vučković, Photon Blockade in Weakly Driven Cavity Quantum Electrodynamics Systems with Many Emitters, *Phys. Rev. Lett.* **122**, 243602 (2019).
- [32] M. A. Carroll, G. D'Alessandro, G. L. Lippi, G.-L. Oppo, and F. Papoff, Thermal, Quantum Antibunching and Lasing Thresholds from Single Emitters to Macroscopic Devices, *Phys. Rev. Lett.* **126**, 063902 (2021).
- [33] J. Tang, L. Tang, H. Wu, Y. Wu, H. Sun, H. Zhang, T. Li, Y. Lu, M. Xiao, and K. Y. Xia, Towards On-Demand Heralded Single-Photon Sources via Photon Blockade, *Phys. Rev. Applied* **15**, 064020 (2021).
- [34] P. F. Yang, X. W. Xia, H. He, S. K. Li, X. Han, P. Zhang, G. Li, P. F. Zhang, J. P. Xu, Y. P. Yang, and T. C. Zhang, Realization of Nonlinear Optical Nonreciprocity on a Few-Photon Level Based on Atoms Strongly Coupled to an Asymmetric Cavity, *Phys. Rev. Lett.* **123**, 233604 (2019).
- [35] X.-X. Hu, Z.-B. Wang, P. F. Zhang, G.-J. Chen, Y.-L. Zhang, G. Li, X.-B. Zou, T. C. Zhang, H. X. Tang, and C.-H. Dong, Noiseless photonic non-reciprocity via optically-induced magnetization, *Nat. Commun.* **12**, 2389 (2021).
- [36] S. Zhang, Y. Hu, G. Lin, Y. Niu, K. Xia, J. Gong, and S. Gong, Thermal-motion-induced non-reciprocal quantum optical system, *Nat. Photonics* **12**, 744 (2018).
- [37] R. H. Lehberg, Radiation from an n -atom system. I. General formalism, *Phys. Rev. A* **2**, 883 (1970).
- [38] K. Xia, M. Macovei, J. Evers, and C. H. Keitel, Robust coherent preparation of entangled states of two coupled flux qubits via dynamic control of the transition frequencies, *Phys. Rev. B* **79**, 024519 (2009).
- [39] K. Xia, M. Macovei, and J. Evers, Stationary entanglement in strongly coupled qubits, *Phys. Rev. B* **84**, 184510 (2011).
- [40] S.-B. Zheng and G.-C. Guo, Efficient Scheme for Two-Atom Entanglement and Quantum Information Processing in Cavity QED, *Phys. Rev. Lett.* **85**, 2392 (2000).
- [41] M. A. Norcia, R. J. Lewis-Swan, J. R. K. Cline, B. Zhu, A. M. Rey, and J. K. Thompson, Cavity-mediated collective spin-exchange interactions in a strontium superradiant laser, *Science* **361**, 259 (2018).
- [42] L. A. Williamson, M. O. Borgh, and J. Ruostekoski, Superatom Picture of Collective Nonclassical Light Emission and Dipole Blockade in Atom Arrays, *Phys. Rev. Lett.* **125**, 073602 (2020).
- [43] A. Cidrim, T. S. do Espirito Santo, J. Schachenmayer, R. Kaiser, and R. Bachelard, Photon Blockade with Ground-State Neutral Atoms, *Phys. Rev. Lett.* **125**, 073601 (2020).
- [44] E. V. Goldstein and P. Meystre, Dipole-dipole interaction in optical cavities, *Phys. Rev. A* **56**, 5135 (1997).
- [45] Y.-M. Zheng, C.-S. Hu, Z.-B. Yang, and H.-Z. Wu, Photon bunching and anti-bunching with two dipole-coupled atoms in an optical cavity, *Chin. Phys. B* **25**, 104202 (2016).
- [46] C. J. Zhu, K. Hou, Y. P. Yang, and L. Deng, Hybrid level anharmonicity and interference-induced photon blockade in a two-qubit cavity qed system with dipole-dipole interaction, *Photon. Res.* **9**, 1264 (2021).
- [47] A. Goban, C.-L. Hung, J. D. Hood, S.-P. Yu, J. A. Muniz, O. Painter, and H. J. Kimble, Superradiance for Atoms Trapped along a Photonic Crystal Waveguide, *Phys. Rev. Lett.* **115**, 063601 (2015).
- [48] P. Y. Wen, K.-T. Lin, A. F. Kockum, B. Suri, H. Ian, J. C. Chen, S. Y. Mao, C. C. Chiu, P. Delsing, F. Nori, G.-D. Lin, and I.-C. Hoi, Large Collective Lamb Shift of Two Distant Superconducting Artificial Atoms, *Phys. Rev. Lett.* **123**, 233602 (2019).
- [49] P. Samutpraphoot, T. Dordević, P. L. Ocola, H. Bernien, C. Senko, V. Vuletić, and M. D. Lukin, Strong Coupling of Two Individually Controlled Atoms via a Nanophotonic Cavity, *Phys. Rev. Lett.* **124**, 063602 (2020).
- [50] C. Song, K. Xu, W. Liu, C.-P. Yang, S.-B. Zheng, H. Deng, Q. Xie, K. Huang, Q. Guo, L. Zhang, P. Zhang, D. Xu, D. Zheng, X. Zhu, H. Wang, Y.-A. Chen, C.-Y. Lu, S. Y. Han, and J.-W. Pan, 10-Qubit Entanglement and Parallel Logic Operations with a Superconducting Circuit, *Phys. Rev. Lett.* **119**, 180511 (2017).
- [51] E. Urban, T. A. Johnson, T. Henage, L. Isenhower, D. D. Yavuz, T. G. Walker, and M. Saffman, Observation of Rydberg blockade between two atoms, *Nat. Phys.* **5**, 110 (2009).
- [52] O. Morin, M. Körber, S. Langenfeld, and G. Rempe, Deterministic Shaping and Reshaping of Single-Photon Temporal Wave Functions, *Phys. Rev. Lett.* **123**, 133602 (2019).

- [53] R. H. Dicke, Coherence in spontaneous radiation processes, *Phys. Rev.* **93**, 99 (1954).
- [54] M. Tavis and F. W. Cummings, Exact solution for an n -molecule—Radiation-field Hamiltonian, *Phys. Rev.* **170**, 379 (1968).
- [55] S. B., D. P. DiVincenzo, and D. Loss, Schrieffer-Wolff transformation for quantum many-body systems, *Ann. Phys.* **326**, 2793 (2011).
- [56] J. R. Schrieffer and P. A. Wolff, Relation between the anderson and Kondo Hamiltonians, *Phys. Rev.* **149**, 491 (1966).
- [57] K. Xia and J. Twamley, All-Optical Switching and Router via the Direct Quantum Control of Coupling between Cavity Modes, *Phys. Rev. X* **3**, 031013 (2013).
- [58] P. Domokos and H. Ritsch, Collective Cooling and Self-Organization of Atoms in a Cavity, *Phys. Rev. Lett.* **89**, 253003 (2002).
- [59] A. Meldrum, P. Bianucci, and F. Marsiglio, Modification of ensemble emission rates and luminescence spectra for inhomogeneously broadened distributions of quantum dots coupled to optical microcavities, *Opt. Express* **18**, 10230 (2010).
- [60] T. Holstein and H. Primakoff, Field dependence of the intrinsic domain magnetization of a ferromagnet, *Phys. Rev.* **58**, 1098 (1940).
- [61] K. Xia and J. Twamley, Generating spin squeezing states and Greenberger-Horne-Zeilinger entanglement using a hybrid phonon-spin ensemble in diamond, *Phys. Rev. B* **94**, 205118 (2016).
- [62] K. Xia, Squeezing giant spin states via geometric phase control in cavity-assisted raman transitions, *Sci. Rep.* **7**, 12836 (2017).
- [63] Z. G. Yan, Y.-R. Zhang, M. Gong, Y. L. Wu, Y. R. Zheng, S. W. Li, C. Wang, F. T. Liang, J. Lin, Y. Xu *et al.*, Strongly correlated quantum walks with a 12-qubit superconducting processor, *Science* **364**, 753 (2019).
- [64] D. Kleppner, Inhibited Spontaneous Emission, *Phys. Rev. Lett.* **47**, 233 (1981).
- [65] J. A. Mlynek, A. A. Abdumalikov, C. Eichler, and A. Wallraff, Observation of Dicke superradiance for two artificial atoms in a cavity with high decay rate, *Nat. Commun.* **5**, 5186 (2014).
- [66] K. Mølmer, Y. Castin, and J. Dalibard, Monte Carlo wave-function method in quantum optics, *J. Opt. Soc. Am. B* **10**, 524 (1993).
- [67] C. W. Gardiner, A. S. Parkins, and P. Zoller, Wave-function quantum stochastic differential equations and quantum-jump simulation methods, *Phys. Rev. A* **46**, 4363 (1992).
- [68] H. Carmichael, *An Open Systems Approach to Quantum Optics*, Vol. 18 (Springer Science & Business Media, New York, 2009).
- [69] G. Crowder, H. Carmichael, and S. Hughes, Quantum trajectory theory of few-photon cavity-QED systems with a time-delayed coherent feedback, *Phys. Rev. A* **101**, 023807 (2020).
- [70] P. Zoller, M. Marte, and D. F. Walls, Quantum jumps in atomic systems, *Phys. Rev. A* **35**, 198 (1987).
- [71] R. Huang, A. Miranowicz, J.-Q. Liao, F. Nori, and H. Jing, Nonreciprocal Photon Blockade, *Phys. Rev. Lett.* **121**, 153601 (2018).
- [72] J. R. Johansson, P. D. Nation, and F. Nori, QuTiP 2: A python framework for the dynamics of open quantum systems, *Comput. Phys. Commun.* **184**, 1234 (2013).
- [73] K. A. Fischer, K. Müller, K. G. Lagoudakis, and J. Vučković, Dynamical modeling of pulsed two-photon interference, *New J. Phys.* **18**, 113053 (2016).
- [74] L. Tang, J. Tang, W. Zhang, G. Lu, H. Zhang, Y. Zhang, K. Xia, and M. Xiao, On-chip chiral single-photon interface: Isolation and unidirectional emission, *Phys. Rev. A* **99**, 043833 (2019).
- [75] Z. Meir, O. Schwartz, E. Shahmoon, D. Oron, and R. Ozeri, Cooperative Lamb Shift in a Mesoscopic Atomic Array, *Phys. Rev. Lett.* **113**, 193002 (2014).
- [76] V. M. Acosta, A. Jarmola, E. Bauch, and D. Budker, Optical properties of the nitrogen-vacancy singlet levels in diamond, *Phys. Rev. B* **82**, 201202(R) (2010).
- [77] J. R. Maze, A. Gali, E. Togan, Y. Chu, A. Trifonov, E. Kaxiras, and M. D. Lukin, Properties of nitrogen-vacancy centers in diamond: The group theoretic approach, *New J. Phys.* **13**, 025025 (2011).
- [78] Ph. Tamarat, N. B. Manson, J. P. Harrison, R. L. McMurtrie, A. Nizovtsev, C. Santori, R. G. Beausoleil, P. Neumann, T. Gaebel, F. Jelezko, P. Hemmer, and J. Wrachtrup, Spin-flip and spin-conserving optical transitions of the nitrogen-vacancy centre in diamond, *New J. Phys.* **10**, 045004 (2008).
- [79] K. Xia and J. Twamley, Solid-state optical interconnect between distant superconducting quantum chips, *Phys. Rev. A* **91**, 042307 (2015).
- [80] K. Xia, N. Zhao, and J. Twamley (EQuS Collaboration), Detection of a weak magnetic field via cavity-enhanced faraday rotation, *Phys. Rev. A* **92**, 043409 (2015).
- [81] Y. Matsuzaki, X. Zhu, K. Kakuyanagi, H. Toida, T. Shimooka, N. Mizuochi, K. Nemoto, K. Semba, W. J. Munro, H. Yamaguchi, and S. Saito, Improving the lifetime of the nitrogen-vacancy-center ensemble coupled with a superconducting flux qubit by applying magnetic fields, *Phys. Rev. A* **91**, 042329 (2015).
- [82] H. Choi, M. Heuck, and D. Englund, Self-Similar Nanocavity Design with Ultrasmall Mode Volume for Single-Photon Non-linearities, *Phys. Rev. Lett.* **118**, 223605 (2017).
- [83] M. Steiner, H. M. Meyer, J. Reichel, and M. Köhl, Photon Emission and Absorption of a Single Ion Coupled to an Optical-Fiber Cavity, *Phys. Rev. Lett.* **113**, 263003 (2014).
- [84] J. Tang, Y. Wu, Z. K. Wang, H. Sun, L. Tang, H. Zhang, T. Li, Y. Lu, M. Xiao, and K. Xia, Vacuum-induced surface-acoustic-wave phonon blockade, *Phys. Rev. A* **101**, 053802 (2020).
- [85] M. Fox, *Quantum Optics: An Introduction* (Oxford University Press, Oxford, 2006).
- [86] D. Hunger, T. Steinmetz, Y. Colombe, C. Deutsch, T. W. Hänsch, and J. Reichel, A fiber Fabry–Perot cavity with high finesse, *New J. Phys.* **12**, 065038 (2010).
- [87] J. Tang, W. D. Geng, and X. L. Xu, Quantum interference induced photon blockade in a coupled single quantum dot-cavity system, *Sci. Rep.* **5**, 9252 (2015).
- [88] A. Faraon, I. Fushman, D. Englund, N. Stoltz, P. Petroff, and J. Vučković, Coherent generation of non-classical light on a chip via photon-induced tunnelling and blockade, *Nat. Phys.* **4**, 859 (2008).